A Bivariate Statistical Technique with Knowledge-based Analytical Hierarchy Process for Landslide Susceptibility Assessment in Naryn River Basin, Kyrgyzstan

Pamirbek kyzy, M.,[1,2,3,4] Kurban, A.,[1,2,3,4]* Strobl, J.,[5] Amanambu, A. C.,[1,2,7] Khan, G.[1,2,6] and Valentine, M.[1,2,3,4]

[1] Xinjiang Institute of Ecology and Geography, Chinese Academy of Sciences, Urumqi 830011, China,
E-mail: merim90@list.ru, alishir@ms.xjb.ac.cn, jonesamanambu@yahoo.com, valensmk@gmail.com

[2] University of Chinese Academy of Sciences, Beijing 100039, China

[3] Research Center for Ecology and Environment of Central Asia, Chinese Academy of Sciences, Urumqi 830011, China

[4] Sino-Belgian Joint Laboratory for Geo-information, Xinjiang Institute of Ecology and Geography and Ghent University, Urumqi 830011, China

[5] University of Salzbury Department of Geoinformatics-Z_GIS. Austrian Academy of Sciences/GIS Science Commission, Austria, E-mail: Josef.Strobl@sbg.ac.at

[6] Karakoram International University, Gilgit, Pakistan, E-mail: gareewwf@mail.com

[7] Water, Engineering and Development Center, School of Civil and Building Engineering, Loughborough University, Leicestershire, UK

*Correspondence Author

Abstract

The model (Frequency Ratio and Pairwise Comparison) used statistical analysis for eight causal factors (slope, curvature, elevation, TWI, NDVI, NDSI, land cover, precipitation) of landslide occurrence. All factors were weighted to apply two-dimensional statistical method of a knowledge-based analytic hierarchical process with data extracted from the spatial database and then converted into a map. Final susceptibility maps showed a close agreement between the two models. The models predicted 72.1% and 69% of the empirical data used for the analysis respectively. These maps can be used to demonstrate the effectiveness of two-dimensional statistical model through the relationship between each factor with a resultant landslide susceptibility. The proposed model can be used to reproduce the relationship between each conditional factor without having to resort to multivariate statistics. The models are a powerful tool for assessing natural hazards, and to produce landslide probability maps for a better definition of risk zones.

1. Introduction

Cataclysmic events have radically increased in recent decades. The international community and government organizations are worried about the loss of human life and ecological damage to properties caused by extreme events (Guzzetti et al., 1999 and Shalaby and Tateishi, 2007). Natural hazards have been globally growing to around 9% of the catastrophic events overall. Statistics from the Center for Research on the Epidemiology of Disasters (CRED) demonstrate that landslides are accountable for at least 17% of all natural hazard fatalities worldwide (Pourghasemi et al., 2012). This is enhanced by progressing deforestation and increased regional precipitation in avalanche risk zones due to changing climate (Yilmaz, 2009 and Brabb and Pampeyan, 1972). Climate change, rising temperatures, severe rains, melting glaciers, all these factors lead to an increase in landslides and negatively affect the lives of individuals and the environment. (Parmesan and Yohe, 2003, Allen et al., 2010 and Change, 2014). A general analysis of landslide events has a long history in Kyrgyzstan. Inventories of landslides and local landslide disasters are documented on the website of the Ministry of Emergency Situations of Kyrgyzstan and several scientific publications. On April 29, 2017, in the village of Ayuu, Osh Oblast, a landslide with a volume of 1 million cubic meters buried 24 people alive. The tragedy was as a result of one of landslides, which is the largest in recent years.

However, this is not the first case in Kyrgyzstan, when a landslide causes the death of people. About 34 Kyrgyz people were buried alive in a 2017 landslide caused by a geological phenomenon (Barra

et al., 2016 and Havenith et al., 2015). According to the report of United Nations Office for Disaster Reduction (UNISDR) Sub-Regional Office for Central Asia and Caucasus approximately 5000 landslides have been identified in the country during 1988 to 2007 where about more than 500 settlments are located hazardous areas. Contrasted with the customary landslide methods, spatial avalanche surveillance and forecast is more helpful and efficient due to innovation in Geographical Information Systems (GIS) and statistical techniques (Wan and Chang, 2014, Yu and Chen, 2017 and Yu et al. 2016). Previously, for the compilation of a map of landslides, simple methods were used (Sarkar and Kanungo, 2004 and Mondini et al., 2017). At the moment, with the progress of GIS, it is possible to compile hazard maps with the use of high-resolution remotely sensed images and statistical analysis, developing an index of landslide susceptibility.

In this scientific work, several factors are considered that can be involved in the formation of landslide. Several specialists have utilized information-driven strategies, different models with statistics index such as frequency ratio (FR), evidential belief function (EBF), frequency ratio weights-of-evidence, logistical regression, artificial neural networks, and analytical hierarchy process (Shahabi et al., 2014, Bui et al., 2011 and Wang et al., 2013). The main difference between this research and the approaches described in the aforementioned publications is a GIS-based analysis resulting in a landslide susceptibility map covering the study area

(Althuwaynee et al. 2014, Akgun, 2012, Lee et al., 2013, Mohammady et al., 2012 and Pourghasemi and Beheshtirad, 2015).

2. Study Area

The study area (Figure 1) is located in the Naryn river basin, the North-Western part of inner Tien-Shan, it covers approximately 31560 km², with altitude 3200m above sea level(asl). The average temperature in winter is -15°C, in summer +30°C. The average amount of precipitation is 350-370 mm with 250-500 mm in mountain regions. Across the study area, slopes are a key natural factor for landslide risk. In this mountain, massif occurs coverslips, caused by shear stress acting parallel to a slide surface. When tensile values exceed the ultimate tensile strength, a cracked shape is formed. The second stage of the landslide process is the formation of the landslide body. The process of landslide formation is irreversible. Therefore, the prognosis for the development of this process is one of the most important problems in the development of mountain regions. As a result of studies of landslide processes in the Naryn river basin, major natural features are identified, in which landslides develop (Barataliev 2010).

Regional contributing features include geology, geomorphology, soil type, recent tectonic movements, climate and seismicity of the region. The main parameters of these factors are established for landslide processes taking place.
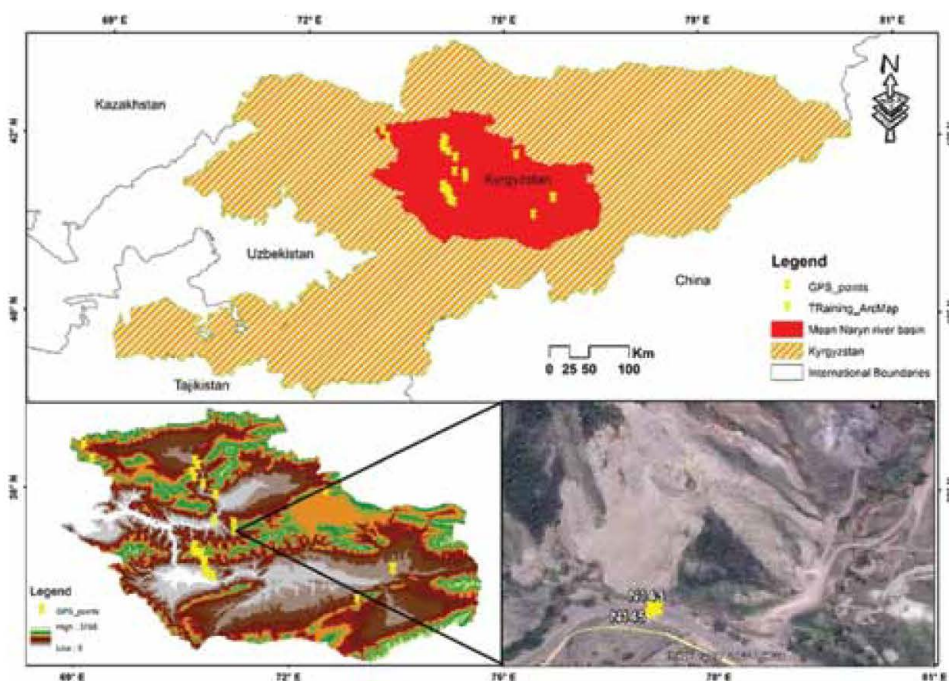

Figure 1: Study area

A geological feature of the development of landslides in this territory is the spread of the Mesozoic-Neozoic rocks, and the indigenous rocks of predominantly Cretaceous age showing slips. Landslides primarily occur at 1000 to 3500m asl. The presence of edges, horsts, wings of tectonic folds and water-bearing faults in the structure of the slope is a tectonic feature of the landslide hazard of this territory. The predominant type of soil in this region is mountain meadow and mountain meadow-steppe soils. These are original types of mountain soils. They are formed under conditions of a large amount of precipitation affecting meadow motley grass of alpine and subalpine types on various soil-forming rocks. The structural mechanism in these soils is coagulative (precipitation of humus-clay-ferruginous complexes) and biogenic. The climate plays a significant role in the development of landslide processes. If during the year the amount of precipitation exceeds 500mm, in combination with other factors this leads to the frequent occurrence of landslides in this region. Local indicators of the danger of a landslide are inherent in a certain degree of slope.

This is the presence of traces of the palaeolithic strata since up to 70% of landslides form on the body of ancient deposits. A high level of groundwater relative to the sliding surface of the landslide and its height of 30-40 cm per day for 6-7 days is a hydrogeological sign of the landslide danger of this slope. The properties of soil coverage are the main factor in the formation and development of a landslide. The presence of more than 50% of clay fraction in soil formations and with soil moisture exceeding 26% is a sign of significant risk of landslides. One of the main features of the landslide hazard is the geomechanical state of the coverslips on the mountain slopes.

3. Data and Methods

The spatial correlation between prediction factors and the dependent factors were calculated whereby the study considered eight conditioning factors (slope, elevation, curvature, land cover, precipitation, NDVI, NDSI and TWI), and the correlation between the predictions where calculated. ESRI ArcMap and Microsoft Excel were used to produce the landslide susceptibility map and thereafter, a validation of the prediction accuracy was done using the common statistical method of Area Under the Curve (AUC).

3.1. Model Application Requirement

To apply the model (FR and PW), dependent factors and independent factors were required. The dependent factors are prediction target location events (landslide, wells and minerals test sites), whereas the independent factors are predictors (predisposing factors). Moreover, the conditioning factors such as the parameters of slope angle, soil type and land use were also taken into consideration. With these factors, the identification and mapping of a set of dependent (target) and independents factors that are directly or indirectly correlated were completed and thereafter the relative contribution of these independents factors in the prediction of dependent factor were estimated (Table 1). An ASTER DEM of the study area was downloaded from the Earth Explorer website https://earthexplorer.usgs.gov, in addition, Landsat 8 ETM/OLI from http://glovis.usgs.gov. Image files were combined into one coverage using the mosaic functionality of ENVI 5.1 software. The Advanced Spaceborne Thermal Emission Reflection Radiometer (ASTER) DEM of study area provides a 30×30 m pixel size.

Table 1: Landslide inventory

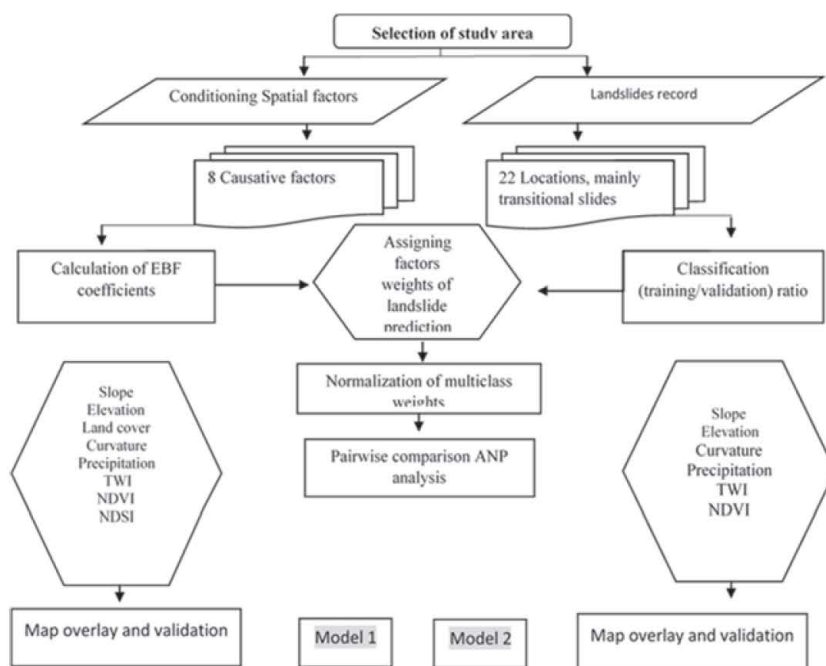| No.	Latitude(N)	Longitude(E)	Elevation(m)	Height of Landslide(m)	Width of Landslide(m)	Slope of Landslide surfase(°)
143	41.40496	74.25377	6321	328	19	48
150	41.42397	74.20401	5656	276	18	50
151	41.48142	74.17505	4845	439	34	35
148	41.50063	74.19118	4849	507	44	50
154	41.54280	74.16222	6559	66	41	55
155	41.54529	74.13541	5369	441	34	55
156	41.55140	74.11471	5513	123	22	45
157	41.55266	74.11003	5661	154	14	62
158	41.56160	74.09396	5730	67	19	64
161	41.59591	74.10186	5964	150	44	56
163	42.05362	74.07215	6528	176	20	51
166	41.58384	74.09493	5865	70	24	50
168	41.20369	73.39219	7053	278	10	25

Figure 2: Processing diagram

The projection of the resulting DEM was established in WGS84_UTM zone43 N, for accurate estimation of a slope layer and various parameters. The program ArcGIS is used to carry out most of the processes (Figure 2).

3.2 Environmental Factors for Models

Land cover: Land cover factor (D) from initial processing of satellite imagery was applied to all datasets (Figure 3). The images were geometrically, radio-metrically and geographically calibrated and corrected. An orthogonal correction was made to avoid mistakes related to topography and landscape analysis affecting water. The satellite image shows low contrast due to a large range of spectral sensitivity. Therefore satellite data were enhanced for better visual interpretation and retrieval of information using both individual and multiband methods (Mei et al., 2016 and El-Zeiny and El-Kafrawy 2017). The vegetation types considered in this study were classified into five groups. Preliminary experiments showed that the vegetation indices in each group had similar spatial and statistical characteristics and provided similar detection of change. Calculation for experimental vegetation index is given below. Formulas and the parameters were based on (Richardson and Everitt 1992 and Lyon et al. 1998). Normalized Differential Vegetation Index (NDVI):

$$NDVI = \frac{(NIR-RED)}{(NIR+RED)}$$

Equation 1

The Normalized Difference Soil Index (NDSI) is an empirical approach for deriving soil information from vegetation and impermeable surface areas. NDSI was developed by dividing the normalized soil index difference of Landsat bands 7 and 2 using brightness as a soil measure, computed for the analysis of land cover change using the band ratio method implemented in ArcGIS (raster calculator) applied to Landsat imagery (Lee and Pradhan 2006, Wang et al., 2002 and Mwaniki et al. 2015). Normalized Differential Soil Index (NDSI):

$$NDSI = \frac{(SWIR2-GREEN)}{(SWIR2+GREEN)}$$

Equation 2

Precipitation: climate data showing average monthly precipitation were derived by interpolating each GPS location obtained from fieldwork. The GPS points were used to reference climatic data from the Climatic Research Unit (CRU TS 4.01) 2011-2016 database (*http://www.cru.uea.ac.uk*) for the summer period from 2011 to 2016. The data from meteorological stations were then transferred, for each location, separately using the Matlab program, and then interpolated for the extent of the study site (39°75-42°75′ N / 72°75′-74°75′ E).

DEM: Figure 3. The topography is used to identify the surface soil conditions.Consequently, the topography represents the surface soil lithology.

Elevation and slope were also included to describe the local conditions and to show the effect of surface geology contrast. If the area is a landslide active region, all considered parameters provide weights to the final local value of the potential index (Ahmad and Singh, 2017 and Montesano et al., 2017). The output of the curvature function can be used to describe the physical characteristics of a drainage basin in order to understand erosion and runoff processes. The profile curvature affects the acceleration and deceleration of surface flow and, consequently, affects erosion. The planar curvature affects the convergence and divergence of the flow. Topographic Wetness Index (TWI) indicators are widely used to approximate the characteristics of soil moisture. The computing method of TWI uses a ratio index method calculating TWI from the DEM (Sörensen et al., 2006). Flow direction and flow accumulation are extracted from DEM using hydrological tools from the Spatial Analyst extension of ArcGIS 10.2. Equation 1 is used for extraction of TWI:

$$TWI = \left(\frac{\alpha}{\tan(\beta)} \right)$$

<div align="right">Equation 3</div>

Where α value is (flow accumulation +1)*slope, β is slope radian.
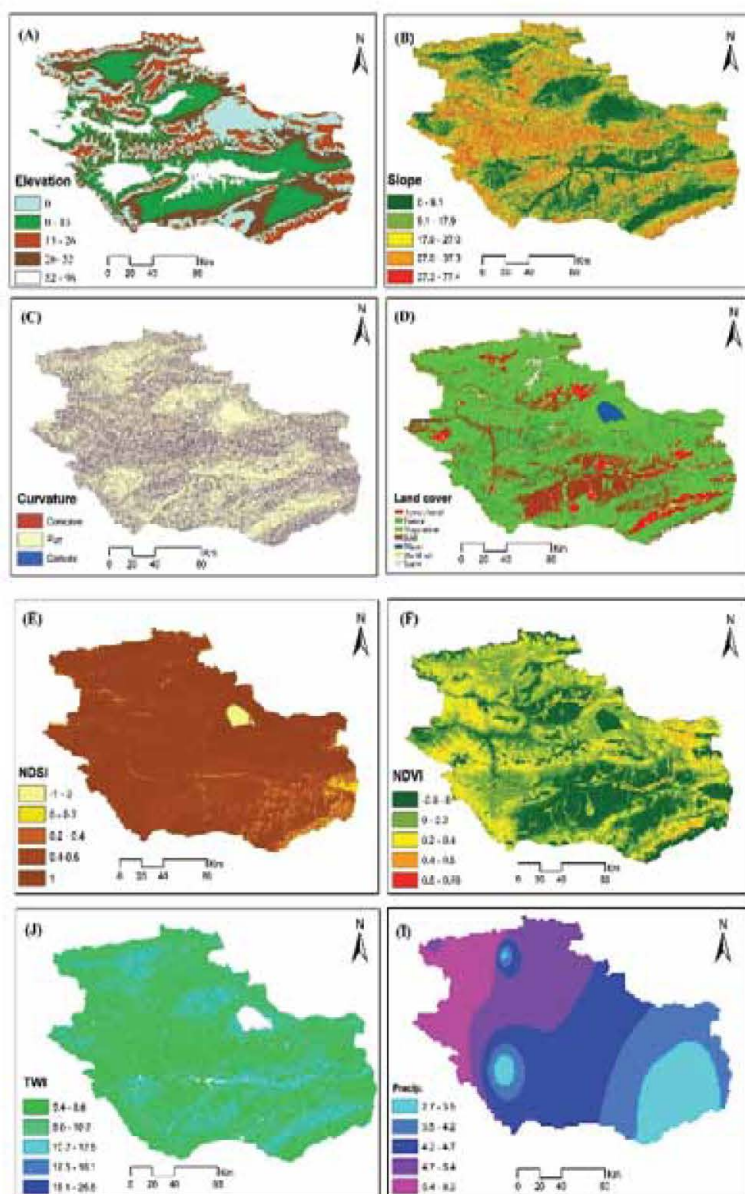

Figure 3: Factors of the model

3.3. The Spatial Prediction using Modified Bivariate Frequency Ratio

The spatial correlation between prediction factors and the dependent factors were calculated, considering eight conditioning factors (slope, elevation, curvature, land cover, precipitation, NDVI, NDSI and TWI) and the correlation between these factors were then calculated. ESRI ArcMap and Microsoft Excel were used to produce the landslide susceptibility map, and thereafter a validation of the prediction accuracy was determined using the most common statistical method of AUC. In this paper, Relative Frequency (RF) = relative density index and (RDI) = frequency Ratio (FR) Processing steps:

- Calculating FR, RF, and PR for each factor
- Calculating pairwise comparison
- Producing susceptibility index map

$$Ratio (+) = \frac{\% \ of \ Pionts}{\% \ of \ class \ area}$$

$$R = {Q}/{R}$$

Equation 4

$$RF = \frac{Ratio \ (1,2,3,4,5)}{Ratio \ total}$$

$$RF = {m}/{M}$$

Equation 5

(Q)=% of points
(R)=% of the class area
(m)=ratio
(M)=total ratio

Spatial analysis of spatial factors to measure the spatial relationship between the conditioning factors and the occurrence of landslides were done using binary values. A complete discussion was omitted, and basic information was not provided regarding the derivation of the algorithm since (Althuwaynee et al., 2014) have already discussed some of these procedures (Table 2). Every feature and causal factor carries a different degree of negative or positive impact on the appearance of the slope. Many studies have revealed this relationship in different approaches to data specification and experimental models. The column matrix (Table 3) shows the pairwise estimates of the relative importance of predictor variables. The predictor factors quantified, serve as input for the pairwise analysis (Ghosh et al. 2011)

$$PR = (RF_{max}-RF_{min})/(RF_{max}-RF_{min})/Min$$

Equation 6

where RF indicates the association of spatial factors. Prediction Rate (PR) is a prognostic indicator. The eigenvectors of the matrix were estimated by normalizing the pairing result for each column. Each coefficient of a pair value in a column was divided by the sum of the pair value of a particular column by obtaining its own value. The pairwise estimation of the matrix by estimating the predictors was obtained by pairwise comparison (Table 3).

Given that the integer values were more applicable to the ranking process, the fractional weights were separated by the smallest weight among all the predictor fractions to convert fractional predictors to integer weights. Decimal numbers were also rounded to the nearest fraction (Table 4). When simulating landslide data, the data was divided into two groups: training and validation data sets. Until now, there was no standard approach or method of selection for training and testing landslide observations. This standard relationship depends on the availability and quality of the data. The two main factors for assessing testing/learning are the stability of time and space. Landslide observations are randomly distributed into two spatial groups: a training data group and a forecasting data group. This procedure can be repeated in reverse to check the results of the prediction.

4. Results and Discussion

In accordance with the above mentioned approaches based on statistics and knowledge, the proposed integration methodology was carried out as a bivariate statistical evidential belief function: PW the integration into the knowledge-based statistics model, using all the extracted parameters; FR integration of FR into the model as a multidimensional model using significant nominated parameters (Figure 4). The analysis of the spatial association of the weights and the spatial relationship between the occurrence of landslides and eight factors (slope, curvature, altitude, NDVI, NDSI, TWI, land cover) are listed in Table 3. In this section, we explicitly describe the association results extracted with this method and the weights used for constructing the models (Table 5). In model PW, the effectiveness of the model as a knowledge-based model of spatial factor statistics is based on high subjectivity.

Table 2: Class weight is figuring of the spatial variables, spatial factors components and the indicators Prediction Rate (PR) in view of the degrees of the spatial affiliation

65-76

A Bivariate Statistical Technique with Knowledge-based Analytical Hierarchy Process for Landslide Susceptibility Assessment in Naryn River Basin, Kyrgyzstan

Factors	Ratio(+)	RF	minRF	maxRF	maxRF-minRF	total minRF	PF
Slope	1.165091	0.243037	0.128909	0.274421	0.145512	0.18409	0.79044
	1.315543	0.274421					
	0.759489	0.158429					
	0.617975	0.128909					
	0.935787	0.195204					
NDVI	0.020884	0.001803	0.001803	0.770133	0.76833	0.001803	4.173669
	8.922392	0.770133					
	1.580777	0.136444					
	0.713024	0.061544					
	0.348446	0.030076					
		0.770133					
Elevation	2.840992	0.527833	5.950081	0.527833	11.27266	5.950081	61.23452
	1.386272	0.257558					
	0.401445	0.074585					
	0.753339	0.139964					
	0.00032	5.95E-05					
		0.527833					
Land cover	3.024596	0.464316	0	0.464316	0.464316	0	2.522225
	0.278864	0.042809					
	1.228069	0.188525					
	1.98256	0.30435					
	0	0					
Curvature	1.501447	0.463138	0.256177	0.463138	0.206961	0.256177	1.124237
	0.909954	0.280685					
	0.830501	0.256177					
NDSI	1.707925	0.307316	0.092777	0.307316	0.214538	0.092777	1.165399
	0.515616	0.092777					
	1.031232	0.185555					
	1.018637	0.183289					
	1.28415	0.231064					
TWI	0.63565	0.099301	0.099301	0.476078	0.376777	0	2.0467
	0.723448	0.113016					
	0.805809	0.125883					
	1.188856	0.185722					
	3.047495	0.476078					
Precipitation	0.63565	0.099301	0.099301	0.476078	0.376777	0	2.0467
	0.723448	0.113016					
	0.805809	0.125883					
	1.188856	0.185722					
	3.047495	0.476078					

Table 3: Column matrix of pairwise ratings of the relative importance of predictors

Predictors	Curvature	Elevation	Slope	TWI	NDVI	Land cover	NDSI	Precipitation
Curvature	1	0.964	0.656	0.549	0.445	0.269	0.246	0.183
Elevation	1.036	1	0.681	0.569	0.462	0.279	0.255	0.191
Slope	1.522	1.468	1	0.836	0.678	0.411	0.375	0.279
TWI	1.821	1.756	1.195	1	0.811	0.491	0.448	0.334
NDVI	2.243	2.164	1.473	1.232	1	0.604	0.553	0.411
Land cover	3.712	3.581	2.438	2.039	1.654	1	0.915	0.681
NDSI	4.054	3.911	2.663	2.227	1.807	1.092	1	0.744
Precipitation	5.446	5.254	3.578	2.991	2.427	1.467	1.343	1

Table 4: Estimated eigenvectors of the row matrix of pairwise rankings and the weight of predictors of susceptibility

PR	Predictors	Curvature	Elevation	Slope	TWI	NDVI	Land cover	NDSI	Precipitation	Fractional weight	Integer weight
Curvature	1.124	0.047	0.047	0.047	0.047	0.047	0.047	0.047	0.047	0.383	1.124
Elevation	1.165	0.049	0.049	0.049	0.049	0.049	0.049	0.049	0.049	0.397	1.165
Slope	1.711	0.073	0.073	0.073	0.073	0.073	0.073	0.073	0.073	0.584	1.711
TWI	2.046	0.087	0.087	0.087	0.087	0.087	0.087	0.087	0.087	0.698	2.046
NDVI	2.522	0.107	0.107	0.107	0.107	0.107	0.107	0.107	0.107	0.861	2.522
Land cover	4.173	0.178	0.178	0.178	0.178	0.178	0.178	0.178	0.178	1.425	4.173
NDSI	4.558	0.194	0.194	0.194	0.194	0.194	0.194	0.194	0.194	1.556	4.558
Precipitation	6.123	0.261	0.261	0.261	0.261	0.261	0.261	0.261	0.261	2.091	6.123
Sum	1	1	1	1	1	1	1	1	1	1	235

Table 5: Total sum after validation

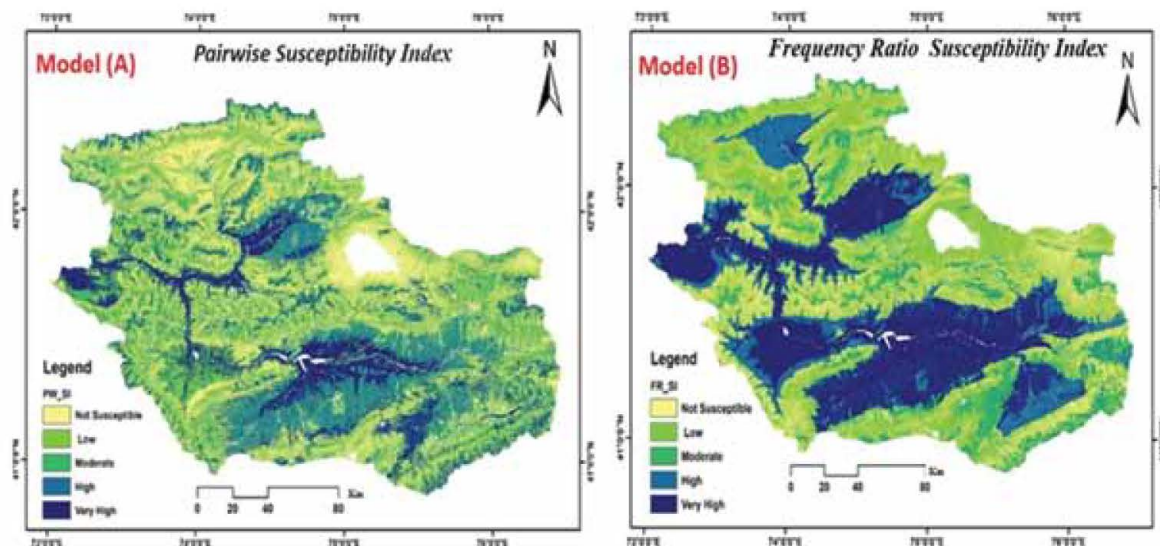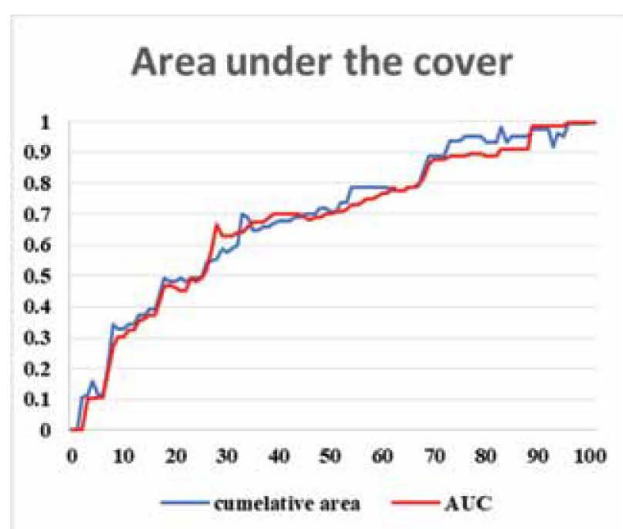| Factors	Prediction using FR	Prediction using PW comparison
Curvature	1.125	0.441
Elevation	1.165	0.459
Slope	1.711	0.672
Twi	2.047	0.804
NDVI	2.522	0.991
land cover	4.173	1.631
NDSI	4.558	1.791
Precipitation	3.062	1.203

Figure 4: Landslide susceptibility models

Figure 5: Landslide susceptibility index rank %

Thus, the weights of PW coefficients are integrated by a pairwise comparison based on the class weights and applied to 8 spatial factors when constructing the results on the success curves. The final map shows that 20% of the study area, where the landslide hazard indicator is ranked highly, containing almost 32% of landslide areas. 67 % of the territory is not affected by landslides. In this study, each factor has exerted positive and non-positive contributions, with some factors generating unique results. FR is based on a two-dimensional statistical method for determining the weights of classes or densities of landslides. The data were normalized. The goal of this method is to transform all real spatial factors for a nonlinear connection (Pereira and Duckstein,

1993_ENREF_21). Six factors in FR were weighted to represent the most significant spatial factors (curvature, elevation, slope, NDVI, precipitatin and TWI prognosis). This study shows that 72% of the study area contains almost all landslides. According to the classification of factors for the two models (Figure 5), land cover PW show the culmination of the relative weight of the factors associated with the actual landslide event, as reflected.

It was also found that the active factors: precipitation, soil moisture, curvature and inclination (and inactive crustal coefficients, height and soil index) are positive and negative (variables in the equation) in the output data table.

Table 6: Validation of Frequency ratio and Pairwise comparison

Method of Validation	Sensitivity class	Number of pixels	Area percent	Landslide percent	Number of Landslide point
Frequency ratio	Not Susceptible	9339741	27.38	8.02	9
	Low	13574908	39.79	1.16	10,1
	Moderate	2943762	8.63	2.53	4
	High	6267115	18.37	5.38	11,12,8,6
	Very high	1983822	5.81	1.70	7, 3,5,6,2
Pairwise comparison	Not Susceptible	6631255	19.52	5.74	4,9
	Low	9325193	27.45	8.00	0
	Moderate	3826629	11.26	3.31	10,2
	High	5855138	17.24	5.07	12,8,
	Very high	8323415	24.50	7.21	3,11,7,5,6

The PW pairwise comparison results and the FR results contain deviations and similarities between the selected factors with respect to the magnitude and sensitivity of the prediction, since the PW is a nonlinear multidimensional model, whereas the paired comparison of FR is based on linear two-dimensional weighing (Ghosh et al., 2011). The results of this study confirm that elevation, curvature and precipitation are common significant factors in the model. The difference between models (PW) and (FR):only six factors were used for the model (FR) (slope, elevation, curvature, precipitation, NDVI and TWI). The model was compiled without the land cover factor, and NDSI. The land cover is nominally scaled and contains several classes and therefore is considered a methodological problem. The NDSI showed a very low weights. The basis of all the weights of the factors was multiplied resulting in a complete cover of all the risk zones. The final maps were divided into five classes of equal intervals (very high, high, medium, low and very low), and seed analysis was performed (Table 6).

6. Conclusion

This study feature methods such as frequency ratio, a bivariate statistical technique using GIS tools and remote sensing data, evaluated in the middle Naryn river basin of Kyrgyzstan. Models FR and PW require a simple process, as well as computational and output processes in comparison with more elaborate models and their statistics. Landslide susceptibility maps obtained in this study showed that a large area is at risk and prone to landslides. The results show that the accuracy of susceptibility using a two-dimensional statistical process based on knowledge by comparing the vulnerabilities of the landslides using FR and PW is of primary importance for landslide susceptibility prediction.

Information provided by this assessment of landslides can help in decision making and mitigation of natural disasters. The model can also be used as a forecast tool since workers and engineers can reduce losses caused by existing and future landslides by preventing, mitigating and preventing exposure to risk.

References

Ahmad, R. A. and Singh, R. P., 2017, Seismic Hazard Assessment of Syria using Seismicity, DEM, Slope, Active Faults and GIS. Remote Sensing Applications: Society and Environment. Vol. 6, 59-70.

Akgun, A., 2012, A Comparison of Landslide Susceptibility Maps Produced by Logistic Regression, Multi-Criteria Decision, and Likelihood Ratio Methods: A Case Study at İzmir, Turkey. *Landslides*. Vol. 9(1), 93-106.

Allen, C. D., Macalady, A. K., Chenchouni, H., Bachelet, D., McDowell, N., Vennetier, M., Kitzberger, T., Rigling, A., Breshears, D. D. and Hogg, E. T., 2010, A Global Overview of Drought and Heat-Induced Tree Mortality Reveals Emerging Climate Change Risks for Forests. Forest Ecology and Management. Vol. 259 (4), 660-684.

Barra, A., Monserrat, O., Mazzanti, P., Esposito, C., Crosetto, M. and Mugnozza, G. S., 2016, First Insights on the Potential of Sentinel-1 for Landslides Detection. *Geomatics Natural Hazards & Risk*. Vol. 7(6), 1874–1883.

Barataliev, O. B., 2010, *The Physical Geography Kyrgyzstan*. Jamaat Press, Bishkek, Kyrgyzstan (original in Kyrgyz language: Кыргызстандын Физикалык Географиясы.)

Brabb, E. E. and Pampeyan, E. H., 1972, Preliminary Map of Landslide Deposits in San Mateo County, California.

Bui, D. T., Lofman, O., Revhaug, I. and Dick, O., 2011, Landslide Susceptibility Analysis in the Hoa Binh Province of Vietnam using Statistical Index and Logistic Regression. *Natural hazards*. Vol. 59(3), 1413.

Change, I. P. O. C., 2014, Climate Change 2014-Impacts, Adaptation and Vulnerability: Regional Aspects: Cambridge University Press.

El-Zeiny, A. and El-Kafrawy, S., 2017, Assessment of Water Pollution Induced by Human Activities in Burullus Lake using Landsat 8 Operational Land Imager and GIS. *The Egyptian Journal of Remote Sensing and Space Science*. Vol. 20, S49-S56.

Guzzetti, F., Carrara, A., Cardinali, M. and Reichenbach, P., 1999, Landslide Hazard Evaluation: A Review of Current Techniques and their Application in A Multi-Scale Study, *Central Italy. Geomorphology*. Vol. 31 (1), 181-216.

Ghosh, S., Carranza, E. J. M., van Westen, C. J., Jetten, V. G. and Bhattacharya, D. N., 2011, Selecting and Weighting Spatial Predictors for Empirical Modeling of Landslide Susceptibility in the Darjeeling Himalayas (India). *Geomorphology*. Vol. 131(1), 35-56.

Havenith, H. B., Strom, A., Torgoev, I., Torgoev, A., Lamair, L., Ischuk, A. and Abdrakhmatov, K., 2015, Tien Shan Geohazards Database: Earthquakes and Landslides. *Geomorphology*. Vol. 249, 16-31.

Lee, S. and Pradhan, B., 2006, Probabilistic Landslide Hazards and Risk Mapping on Penang Island, Malaysia. *Journal of Earth System Science*. Vol. 115(6), 661-672.

Lee, S., Hwang, J. and Park, I., 2013, Application of Data-Driven Evidential Belief Functions to Landslide Susceptibility Mapping in Jinbu, Korea. *Catena*. Vol. 100, 15-30.

Lyon, J. G., Yuan, D., Lunetta, R. S. and Elvidge, C. D., 1998, A change Detection Experiment using Vegetation Indices. *Photogrammetric Engineering and Remote Sensing*. Vol. 64(2), 143-150.

Mei, A., Manzo, C., Fontinovo, G., Bassani, C., Allegrini, A. and Petracchini, F., 2016, Assessment of Land cover changes in Lampedusa Island (Italy) using Landsat TM and OLI Data. *Journal of African Earth Sciences*. Vol. 122, 15-24.

Mohammady, M., Pourghasemi, H. R. and Pradhan, B., 2012, Landslide Susceptibility Mapping at Golestan Province, Iran: A Comparison between Frequency Ratio, Dempster–Shafer, and Weights-of-Evidence Models. *Journal of Asian Earth Sciences*. Vol. 61, 221-236.

Mondini, A. C., Chang, K. T., Chiang, S. H., Schlogel, R., Notarnicola, C. and Saito, H., 2017, Automatic Mapping of Event Landslides at Basin Scale in Taiwan using a Montecarlo Approach and Synthetic Land Cover Fingerprints. *International Journal of Applied Earth Observation and Geoinformation*. Vol. 63, 112-121.

Montesano, P. M., Neigh, C., Sun, G., Duncanson, L., Van Den Hoek, J. and Ranson, K. J., 2017, The use of Sun Elevation Angle for Stereogrammetric Boreal Forest Height in Open Canopies. *Remote Sensing of Environment*. Vol. 196, 76-88.

Mwaniki, M. W., Agutu, N. O., Mbaka, J. G., Ngigi, T. G. and Waithaka, E. H., 2015, Landslide Scar/Soil Erodibility Mapping using Landsat TM/ETM+ Bands 7 and 3 Normalised Difference Index: A Case Study of Central Region of Kenya. *Applied Geography*. Vol. 64, 108-120.

Parmesan, C. and Yohe, G., 2003, A Globally Coherent Fingerprint of Climate Change Impacts Across Natural Systems. *Nature*. Vol. 421(6918), 37-42.

Pereira, J. M. and Duckstein, L., 1993, A Multiple Criteria Decision-Making Approach to GIS-based Land Suitability Evaluation. *International Journal of Geographical Information Science*. Vol. 7(5), 407-424.

Pourghasemi, H. R. and Beheshtirad, M., 2015, Assessment of a Data-Driven Evidential Belief Function Model and GIS for Groundwater Potential Mapping in the Koohrang Watershed, Iran. *Geocarto International*. Vol. 30(6), 662-685.

Pourghasemi, H. R., Mohammady, M. and Pradhan, B., 2012, Landslide Susceptibility Mapping using Index of Entropy and Conditional Probability Models in GIS: Safarood Basin, Iran. *Catena*. Vol. 97, 71-84.

Richardson, A. J. and Everitt, J. H., 1992, Using Spectral Vegetation Indices to Estimate Rangeland Productivity. *Geocarto International*. Vol. 7(1), 63-69.

Sarkar, S. and Kanungo, D., 2004, An Integrated Approach for Landslide Susceptibility Mapping using Remote Sensing and GIS. *Photogrammetric Engineering & Remote Sensing*. Vol. 70(5), 617-625.

Shahabi, H., Khezri, S., Ahmad, B. B. and Hashim, M., 2014, Landslide Susceptibility Mapping at Central Zab Basin, Iran: A Comparison Between Analytical Hierarchy Process, Frequency Ratio and Logistic Regression Models. Catena. Vol. 115, 55-70.

Shalaby, A. and Tateishi, R., 2007, Remote Sensing and GIS for Mapping and Monitoring Land cover and Land-use changes in the Northwestern Coastal Zone of Egypt. *Applied Geography*. Vol. 27(1), 28-41.

Sörensen, R., Zinko, U. and Seibert, J., 2006, On the Calculation of the Topographic Wetness Index: Evaluation of Different Methods Based on Field Observations. *Hydrology and Earth System Sciences Discussions*. Vol. 10(1), 101-112.

UNISDR, 2010, In-depth Review of Disaster Risk Reduction in the Kyrgyz Republic. Secretariat of the United Nations International Strategy for Disaster Reduction Sub - Regional Office for Central Asia and Caucasus.

Wan, S. and Chang, S. H., 2014, Combined Particle Swarm Optimization and Linear Discriminant Analysis for Landslide Image Classification: Application to a Case Study in Taiwan. *Environmental Earth Sciences*. Vol. 72(5), 1453-1464.

Wang, G., Wente, S., Gertner, G. and Anderson, A., 2002, Improvement in Mapping Vegetation Cover Factor for the Universal Soil Loss Equation by Geostatistical Methods with Landsat Thematic Mapper Images. *International Journal of Remote Sensing*. Vol. 23(18), 3649-3667.

Wang, L. J., Sawada, K. and Moriguchi, S., 2013, Landslide Susceptibility Analysis with Logistic Regression Model Based on FCM Sampling Strategy. *Computers & Geosciences*. Vol. 57, 81-92.

Yilmaz, I., 2009, Landslide Susceptibility Mapping using Frequency Ratio, Logistic Regression, Artificial Neural Networks and their Comparison: A Case Study from Kat Landslides (Tokat—Turkey). *Computers & Geosciences*. Vol. 35(6), 1125-1138.

Yu, B. and Chen, F., 2017, A New Technique for Landslide Mapping from a Large-Scale Remote Sensed Image: A Case Study of Central Nepal. *Computers & Geosciences*. Vol. 100, 115-124.

Yu, X., Wang, Y., Niu, R. and Hu, Y., 2016, A Combination of Geographically Weighted Regression, Particle Swarm Optimization and Support Vector Machine for Landslide Susceptibility Mapping: A Case Study at Wanzhou in the Three Gorges Area, China. *International Journal of Environmental Research and Public Health*. Vol. 13(5):487.